# 22. The Self-Recognition and Self-Assembly of Folic Acid Salts in Isotropic Water Solution

by **Giovanni Gottarelli***, **Elisabetta Mezzina***, and **Gian Piero Spada**

Dipartimento di Chimica Organica 'A. Mangini', Università di Bologna, Via S. Donato 15, I–40127 Bologna

and **Flavio Carsughi, Giovanni Di Nicola, Paolo Mariani***, and **Annalaura Sabatucci**

Istituto di Scienze Fisiche, Università di Ancona, Via Ranieri 65, I–60131 Ancona

and **Stefania Bonazzi**

I. Co. C.E.A.-C.N.R., Area della Ricerca di Bologna, Via Gobetti 101, I–40129 Bologna

(20.IX.95)

The self-assembly of alkaline folates in isotropic water solutions, with or without added salts, has been investigated by small-angle neutron-scattering, circular-dichroism, and NMR techniques. The assembled species are chiral, cylindrical aggregates of finite length, composed of stacked tetramers; each tetramer is formed by *Hoogsteen*-bonded folate residues. The assembly process is more efficient in the presence of an excess of $Na^{I}$ ions, leading to longer aggregates with stronger tetramer-tetramer interaction. In pure water, the rods are shorter and the tetramer-tetramer interaction weaker. Association between folates can be detected by circular-dichroism spectroscopy starting from a concentration of $6 \cdot 10^{-4}$ mol $l^{-1}$, well below the critical concentration for the formation of the cholesteric mesophase (*ca.* 0.5 mol $l^{-1}$).

**1. Introduction.** – Self-recognition and self-assembly processes lead to the formation of complex supramolecular structures starting from simple molecules [1]. Although several characterizations of assembled species in the crystal phase are reported in the literature, only a few studies of those in isotropic solutions are available. Guanine-rich oligonucleotides, due to the particular arrangement of H-bond donor and acceptor groups, give rise to unusual tetrameric structures which seem to play important biological roles [2]. Homoguanylic deoxyoligonucleotides form supramolecular aggregates leading to liquid crystalline phases of the hexagonal and cholesteric type [3]. Folic acid ( = *N*-{4-{[(2-amino-1,4-dihydro-4-oxo-6-pteridinyl)methyl]amino}benzoyl}-L-glutamic acid; see *Fig. 1, a*) is an important biologically active molecule characterized by the presence of the pterin nucleus, which has a structure similar to guanine. Recently, we have shown that also alkaline folates, in water, form cholesteric and hexagonal mesophases [4] [5]. The building blocks of these phases are chiral columns composed of a stacked array of folate tetramers similar to guanine tetramers (see *Fig. 1*). In the liquid crystalline phase, pterin molecules are able to self-recognize and self-organize in a similar way to guanosine derivatives. Ions play an important role in this process, and the cholesteric phase is stable only in the presence of an excess of $Na^{I}$ cations.

In this paper we report a study of the self-assembly of alkaline folates in isotropic solution by small-angle neutron scattering (SANS), circular dichroism (CD), and $^{1}$H-NMR.

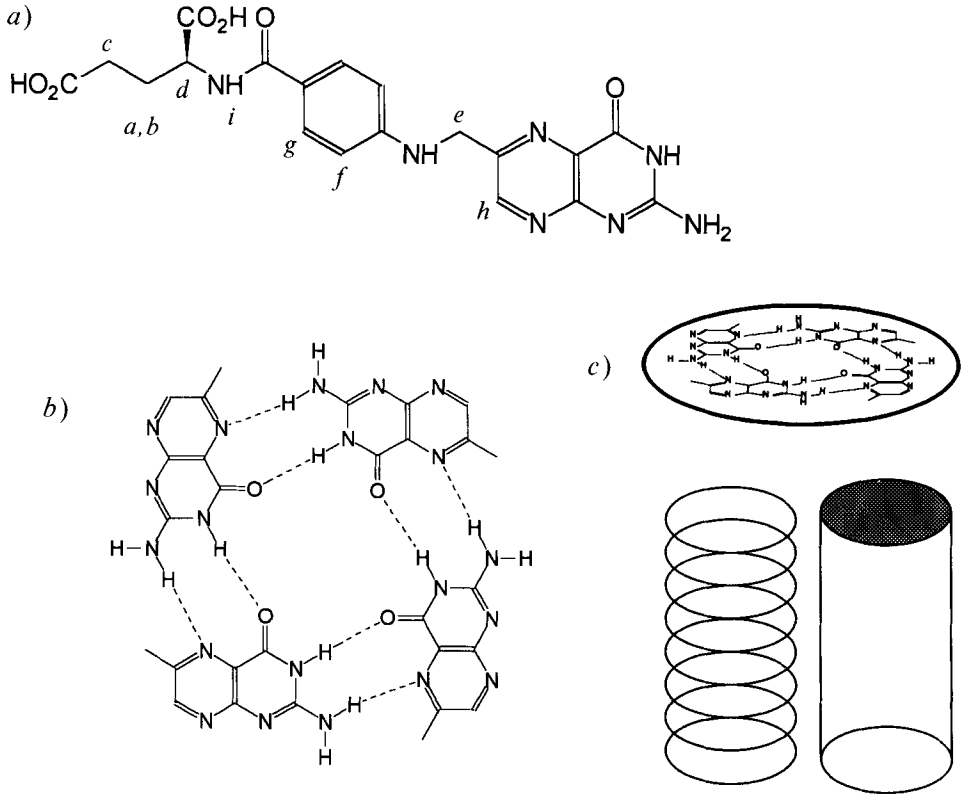


Fig. 1. *Model of formation of the columnar aggregate from folate:* a) *Structure of folic acid,* b) *the* Hoogsteen-*bonded tetrad formed by four pterin units and* c) *the cylinder formed by the piling-up of tetrads*

**2. Results and Discussion.** – 2.1. *Small-Angle Neutron Scattering.* SANS Experiments were carried out to characterize the structural properties of the aggregates in the isotropic solution. In particular, SANS cross sections were measured for $D_2O$ solutions of disodium folate ($Na_2fol$) and dipotassium folate ($K_2fol$), as well as for NaCl (1M) solutions of $Na_2fol$ and KCl (1M) solutions of $K_2fol$. Two folate concentrations were considered, namely 1.5 and 4% (*w/w*). In all cases, $D_2O$ was used as a solvent to reduce the incoherent background and to obtain a better signal-to-noise ratio. The experiments were performed at two different temperatures, *i.e.*, 20 and 10°.

For all the samples investigated at the concentration of 1.5%, both in the presence and in the absence of salts, the SANS profiles do not show any signals, but are characterized by a flat background, typical of incoherent scattering. This finding indicates that, at this concentration, the aggregates possibly present in solution (see CD section) are too small or too few to be detected in the investigated $Q$ range.

Different results were obtained for samples with 4% folate concentration. In *Fig. 2,* the calibrated neutron-scattering intensities observed at 20° are reported: at this concentration, folates dissolved in NaCl and KCl solutions, but not in pure water, show a small-angle scattering signals. The *Guinier* plots $\ln(d\Sigma/d\Omega\ (Q))$ *vs.* $Q^2$ relative to the

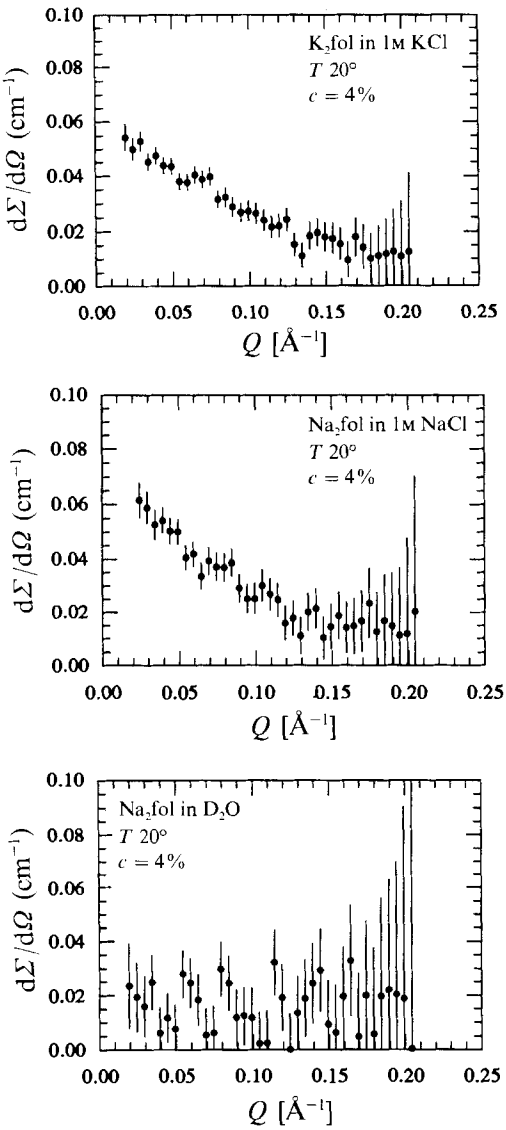


Fig. 2. *Neutron-scattering intensity profiles relative to some of the investigated folate samples* ($c = 4\%$ ($w/w$), $T$ 20°). Data are shown in absolute scale.

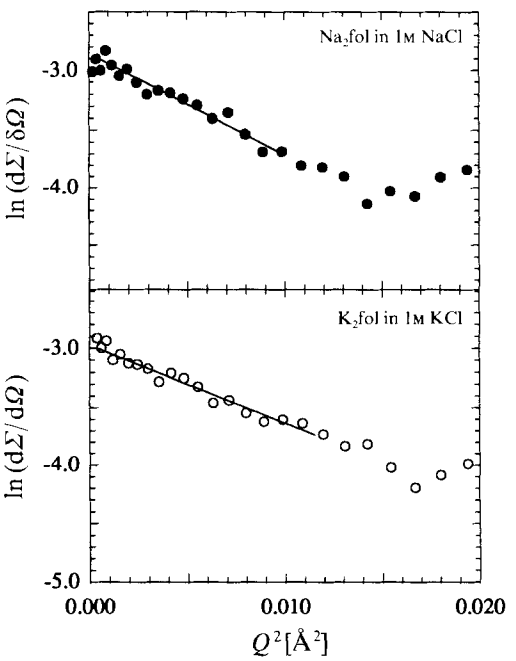


Fig. 3. Guinier *analysis of the scattering curves relative to the folate samples with* c = *4%*. The straight lines correspond to the best fit through the experimental points for which the *Guinier* law is satisfied.

$Na_2$fol in NaCl solution and to $K_2$fol in KCl solution are reported in *Fig. 3*, where the linear behavior up to $QR_g \approx 1.5$ is also shown. The corresponding radii of gyration ($R_g$) and the SANS cross sections at zero angle ($d\Sigma/d\Omega(0)$) are indicated in *Table 1*: it is interesting that both samples show a gyration radius of *ca.* 14 Å, independently of temperature.

Table 1. *SANS Structural Results Obtained at* c = 4%[a])

| | *T* [°] | $R_g$ [Å] | *h* [Å] | *n* | *n** | $d\Sigma/d\Omega(0)$ [$cm^{-1}$] | *N* | Aggregation [%] |
|---|---|---|---|---|---|---|---|---|
| $Na_2$fol or $K_2$fol in $D_2O$ | 10 | – | – | – | – | – | – | 0 |
| | 25 | – | – | – | – | – | – | 0 |
| $Na_2$fol in 1M NaCl | 10 | 14.3±0.8 | 31.8±4.0 | 9.5±1.2 | 8±2 | 0.045±0.003 | $(3.0\pm1.0)\cdot10^{17}$ | 23±11 |
| | 25 | 14.9±0.5 | 35.0±2.5 | 10.4±0.7 | 9±2 | 0.056±0.002 | $(3.1\pm0.5)\cdot10^{17}$ | 26±6 |
| $K_2$fol in 1M KCl | 10 | 13.8±0.5 | 29.0±2.8 | 8.6±0.8 | 8±2 | 0.047±0.002 | $(3.8\pm0.9)\cdot10^{17}$ | 28±9 |
| | 25 | 14.2±0.4 | 31.3±2.2 | 9.3±0.6 | 9±2 | 0.052±0.002 | $(3.6\pm0.6)\cdot10^{17}$ | 29±7 |

[a]) $R_g$ and $d\Sigma/d\Omega(0)$ are the radius of gyration and the coherent intensity scattered at $Q = 0$, respectively, as determined from *Guinier* plots by linearly fitting the experimental points in the low-$Q$ region for which the *Guinier* law is satisfied; *h* and *n* are the height of the model cylindrical particle and the related number of stacked tetramers, respectively, as determined by fitting the observed gyration radius with *Eqn. 2* in the text and by using a radius of 15.5 Å; *n** is the number of stacked tetramers as determined by numerical simulation, by comparing the experimental scattering profile with the profile calculated for a cylinder with radius equal to 15.5 Å and formed by a variable number of disks; *N* is the number of scattering particles per $cm^3$ as determined from *Eqn. 5* by using the cylindrical model particle with radius 15.5 Å and height *h*; the last column reports, as percentage with respect to the nominal sample concentration, the number of molecules which are in an aggregate form.

According to previous SANS measurements in deoxyguanosine systems [6], the basic structure of the scattering particles existing in isotropic solution is assumed to be similar to the one determined for the columns forming the hexagonal and cholesteric phases. A similar hypothesis seems reasonable also in the case of folates: accordingly, the experimental gyration radius could be compared to that of a rod-shaped model: with reference to the structure of the columns, as determined in the mesophases [4] [5], the radius *R* of the scattering cylindrical particle corresponds to the radius of the tetrameric disk. Accordingly, the height of aggregate *h* is related to the number *n* of stacked tetramers by *Eqn. 1* where *d* is the distance between piled disks, determined in the hexagonal phase by X-ray diffraction experiments [4] [5], and the value 6.4 takes into account the hydration of the terminal disks [7]. Therefore, the gyration radius of the rod-shaped model [8] [9] is given by *Eqn. 2*.

$$h = (n - 1)\ d + 6.4 \tag{1}$$

$$R_{g,mod} = [(2R^2 - h^2/3)/4]^{1/2} \tag{2}$$

The comparison is straightforward: the structural data of models which best fit the experimental data are reported in *Table 1*. The length of the cylindrical aggregates is *ca.* 30 Å, which corresponds to the stacking of about 9 disks. It is interesting to observe that, within the experimental error, this result is insensitive to the temperature, as well as to the type of added ions.

We also analyzed the $\ln(d\Sigma/d\Omega(Q)\,Q)$ *vs.* $Q^2$ plots [6] in which a linear behavior in the low $Q$ range is expected in the presence of needle-like scattering particles [8] [10]. However, the result obtained were not unambiguous, so that it was not possible to determine the radius of the cylindrical aggregate cross section. Considering the length of the aggregates with respect to their radius, this result is not surprising: in the present systems, the scattering particles cannot really be assumed to consist of 'extremely elongated' aggregates [10] (see also *Sect. 2.3*).

Confirmation of the validity of the proposed structural model has been obtained from numerical simulations: we calculated the scattering profile from cylindrical objects formed from a variable number of disks [11]. The best agreement between the calculated and the experimental curves was obtained for 8–9 piled disks (*Table 1*).

Other interesting information has been obtained from the analysis of the scattered intensity at zero angle. By using *Eqn.6* (see *Exper. Part*), the number of scattering particles per unit volume could be calculated [9] [12]. As the mean particle composition has been derived from the best-fitting model, it is, therefore, possible to derive the number of molecules which are in an aggregate form per unit volume. This quantity, calculated assuming an H/D exchange parameter of 2.5 [13], is also reported in *Table 1:* comparison with the sample concentration clearly indicates that only a fraction of molecule self-associates in solution, while a second fraction does not form detectable scattering particles or maybe remains in a true monomeric state. This fact is emphasized in *Table 1* by the reported percentage of aggregation.

A last point should be discussed: the length of the scattering particles appears closely related to that of the columnar aggregates in the mesophases. The variation of the average columnar length in the cholesteric and hexagonal phases was previously determined as a function of concentration (see Fig. 9 in [5]): at each concentration, this length was obtained by shape analysis of the characteristic X-ray diffraction peak corresponding to the tetramer stacking [5]. In the case of $Na_2$fol in 1M NaCl and $K_2$fol in 1M KCl, the aggregate length in the mesophases slowly decreases as the water content increases (see Fig. 9 in [5]). For $Na_2$fol in pure water, a strong sensitivity of the columnar length to the concentration was observed, so that close to the I–H phase transition, the columns are formed by only 5 disks. The average number of stacked disks in the isotropic solutions could be tentatively calculated by linear extrapolation of the data reported in Fig. 9 in [5]: at 1.5 and 4% concentration, the piled disks are 8 and 9 in 1M KCl, and 10 and 11 in 1M NaCl, respectively. In water, the presence of aggregates could not be deduced. In fact, at both the investigated concentrations, no scattering particles were detected by SANS.

The absence of small-angle scattering for NaCl and KCl solutions at folate concentration of 1.5% (where the scattering aggregates are predicted to be formed by 8 and 10 piled disks, resp.) could be explained by taking into account the further decrease of the effective concentration of scattering particles, expected by considering the partial molecular aggregation deduced from concentration measurements.

2.2. *Circular Dichroism.* Even if the assignment of the electronic transitions of the pterin chromophore is not available and thus a detailed interpretation of the spectra is not possible, CD spectroscopy can be fruitfully employed as an empirical tool to follow the self-assembly process of the alkaline folates.

Selected spectra recorded for water solution of $Na_2$fol or $K_2$fol at different temperatures and concentrations with and without added salts are reported in *Figs. 4* and *5*. Three basic spectral shapes can easily be identified:

*i*) The first one, corresponding to free folate (*e.g. Fig. 4, a*, thin line), is characterized by a broad positive band centered at *ca.* 280 nm; this spectrum is observed in diluted solutions at room temperature and also under more aggregating conditions at higher temperature.

*ii*) A second spectral shape (*e.g. Fig. 4, a*, thick line) is observed in pure water at 0.4% concentration at room temperature and, in the presence of added salts, also at higher

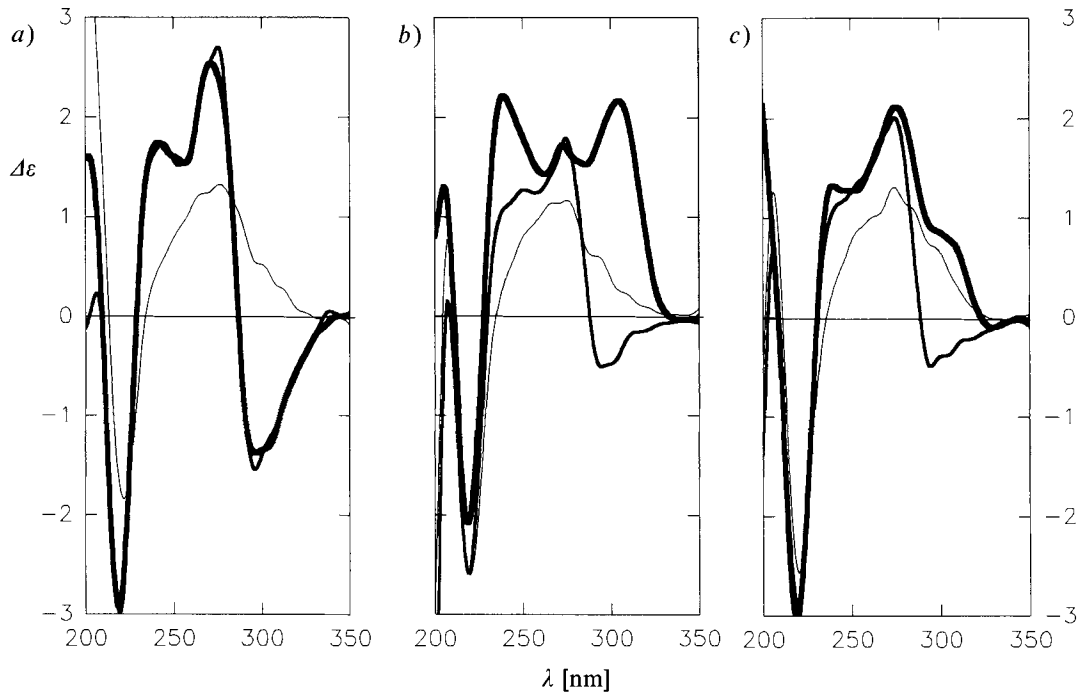


Fig. 4. *Selected CD spectra of folate at concentration* c = *0.4% (w/w)*: a) *spectra of $Na_2$fol in water at 5, 30, and 60°* (thick, medium, and thin lines, resp.); b) *spectra of $Na_2$fol in aqueous 1* M *NaCl at 5, 30, and 60°* (thick, medium, and thin lines, resp.); c) *spectra of $K_2$fol in aqueous 1* M *KCl at 5, 22, and 60°* (thick, medium, and thin lines, resp.)

temperature. It is characterized by a negative band at *ca.* 290 nm and a positive band at *ca.* 270 nm; this spectrum melts to that of the free folate at temperatures which depend on the folate concentration and the amount of added salt. We shall refer to it as corresponding to aggregate form **I**. This spectrum is observed, at room temperature, also for low-concentration (down to 0.03%, $6 \cdot 10^{-4}$ M) solutions with and without NaCl.

*iii*) Finally, a third spectral shape (*e.g. Fig. 5, b*, thick line) is observed at high folate concentration in the presence of NaCl. It is characterized by a positive band at *ca.* 310 nm. It corresponds to an aggregated form which will be referred to as **II**. This third spectrum melts to the second one only at low folate concentration.

A common feature of both assembled species **I** and **II** is a positive band at *ca.* 240 nm whose intensity is stronger in the presence of NaCl. The non-assembled and both the assembled species show also a negative band at *ca.* 220 nm which is little affected by the aggregation process. This band is likely to be related to the amide chromophore and is diagnostic of the configurational events occurring around the glutamic side chain. Furthermore, an inspection of the CD spectra in KCl at both concentrations clearly indicates that we are in the presence of both **II** and **I** forms (the positive band at *ca.* 270 nm, typical of form **I**, is still present).

The melting profiles of the 0.4% solutions with and without added salts are reported in *Fig. 6*. In the presence of salts, a low-temperature melting ($\Delta\varepsilon$ from positive to negative)

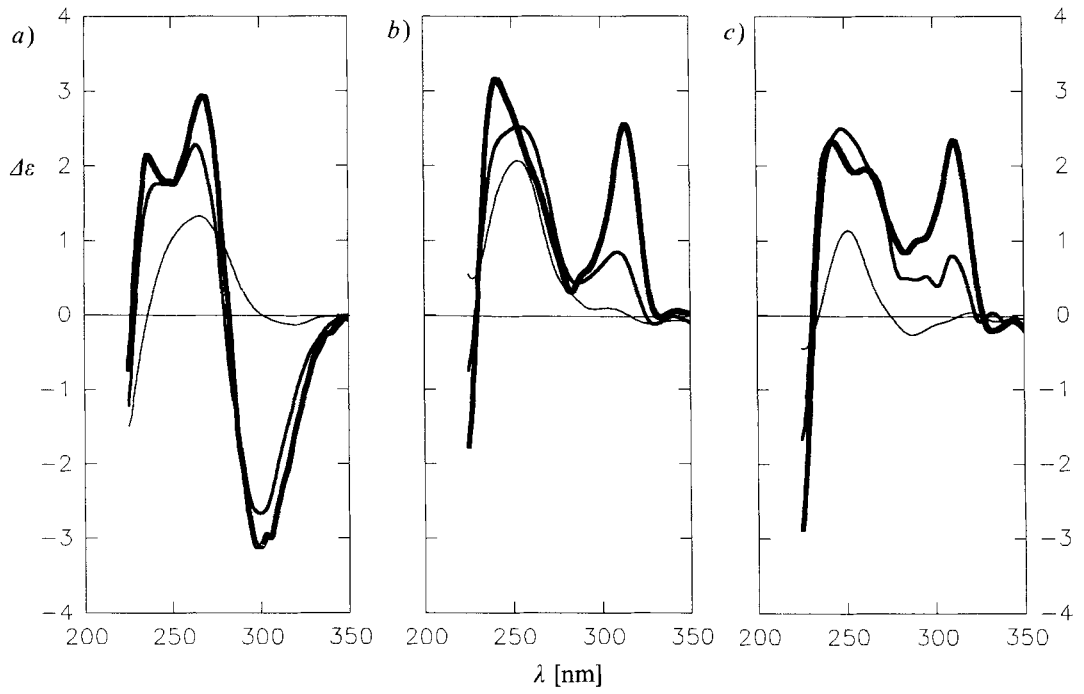


Fig. 5. *Selected CD spectra of folate at concentration* c = *4% (w/w)*: a) *spectra of $Na_2$fol in water at 8, 30, and 75°* (thick, medium, and thin lines, resp.); b) *spectra of $Na_2$fol in aqueous 1 M NaCl at 4, 30, and 70°* (thick, medium, and thin lines, resp.); c) *spectra of $K_2$fol in aqueous 1 M KCl at 4, 30, and 80°* (thick, medium, and thin lines, resp.)

and a higher-temperature shallow melting ($\Delta\varepsilon$ from negative to positive) are observed. In water, only the high-temperature melting is observed. The melting at lower temperature corresponds to the transition **II**→**I** and the one in the presence of $Na^I$ is slightly higher than that in the presence of $K^I$ [1]). The high-temperature melting leads to the free species.

A comparison of the CD results with those from SANS can be made only for 4% solutions in the presence of added ions (form **II**) as, for lower concentrations, SANS is not sensitive enough to detect the associated species. At 4% folate concentration with added NaCl or KCl, SANS results indicate the presence of cylinders composed of 9 stacked tetramers. CD Spectra at 0.4 and 4% in the presence of NaCl are very similar (at 0.4%, the band at 270 nm indicates that also some of aggregate **I** is present); we may conclude that at the lower concentration, the assembled cylinders are either too short or too few to be detected by SANS, but have substantially the same configurational features as those formed at the higher concentration.

---

[1]) The higher stabilization due to the $Na^I$ ions is more evident in relation to the formation of the cholesteric phase (see [5]) which is stable in a measurable concentration interval only in the presence of an excess of $Na^I$ ions. On the other hand, extrapolation of the columnar length obtained in the hexagonal phase to 4% indicate that in the presence of $Na^I$ the columns are slightly longer.

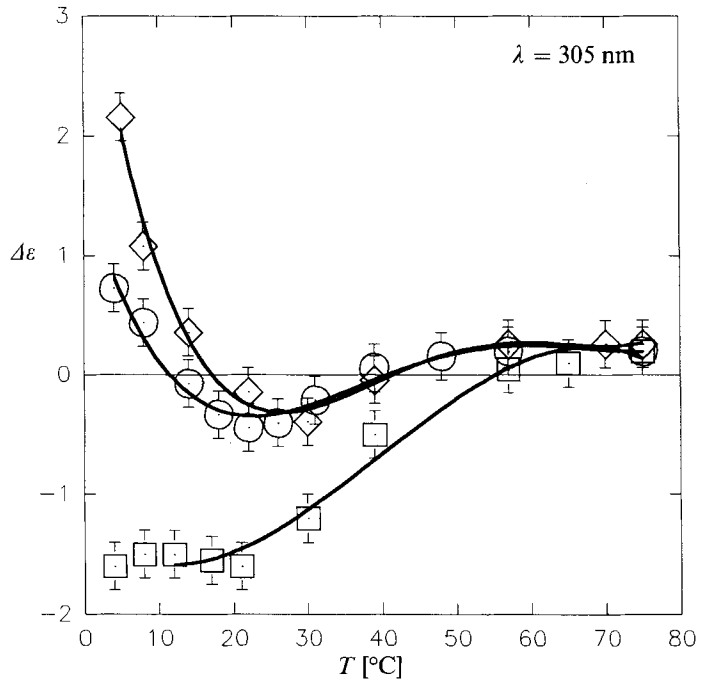


Fig. 6. *The 'melting profile'* ($\Delta\varepsilon$ at 305 nm *vs.* temperature) *of folate solutions at concentration* c = *0.4%* (*w*/*w*). In water, □; in aqueous 1M NaCl, ◇; in aqueous 1M KCl, ○.

We cannot say much about form **I**. CD Spectral features are very different from those of the free molecules. A hexagonal columnar mesophase is formed also in pure water and, from X-ray measurements, the diameter is the same as that detected in NaCl solution. The aromatic stacking distance in pure water is slightly greater than in NaCl solution, particularly at lower concentrations; the extra salt added seems to increase the tetramer-tetramer attractive interactions. Also form **I** could, therefore, be a cylinder composed of stacked tetramers, but less tightly bound to each other than in form **II**.

As reported for guanine derivatives, also in this case, the cation is likely to be in the central cavity between two stacked tetramers, coordinated to the carbonyl O-atoms [14].

Finally, the insensitivity of the amide CD band to aggregation seems to indicate that the process does not substantially affect the glutamic-chain mobility.

2.3. *NMR Structural Analysis.* 2.3.1. *1D-NMR Data. Table 2* collects some $^1$H-NMR data obtained under different conditions and concentrations; the exchangeable protons of the pterin moiety do not appear[2]). An additional signal is detected in spectra of 4%

[2]) This was somehow unexpected, as, in the case of deoxyguanosine derivatives, these signals become detectable when tetrameric structures are formed. The failure in detecting these signals [15] could depend on the pH of the solution which is 8.5–9 and on the presence of the carboxylate ions which could act as a catalyst for proton exchange. Furthermore, the structural variation of pterin with respect to guanine might enhance the acidity of the imino protons, causing a faster proton exchange. On the other hand, the lack of these signals may also depend on a looser structure of the tetramer.

Table 2. *Some $^1$H-NMR Data of Solutions of $Na_2$fol*

| *Entry* | $Na_2$fol | *T* [°] | | $H_h$ | $H_g$ | $H_f$ | $H_e$ | $H_d$ | $H_c$ | $H_{a,b}$ |
|---|---|---|---|---|---|---|---|---|---|---|
| *1* | 0.4% $D_2O$ | 60 | $\delta$ [ppm] | 8.73 (*s*) | 7.68 (*d*, *J* = 8.8 Hz) | 6.80 (*d*, *J* = 8.8 Hz) | 4.61 (br. *s*) | 4.32 (*dd*, *J* = 8.3, 4.4 Hz) | 2.27 (*m*) | 2.21 (*m*), 2.05 (*m*) |
| | | | $T_1$ [s] | 4.37±0.19 | 2.10±0.15 | 1.16±0.03 | 1.26±0.06 | | 1.15±0.07 | 1.00±0.07, 0.66±0.10 |
| *2* | 0.4% $D_2O$ | 20 | $\delta$ [ppm] | 8.68 (*s*) | 7.61 (*d*, *J* = 8.8 Hz) | 6.64 (*d*, *J* = 8.8 Hz) | 4.46 (br. *s*) | 4.31 (*dd*, *J* = 8.7, 4.5 Hz) | 2.33 (*m*) | 2.15 (*m*), 2.04 (*m*) |
| | | | $T_1$ [s] | 1.88±0.05 | 1.10±0.03 | 0.69±0.03 | | | 0.43±0.05 | 0.28±0.02, 0.28±0.02 |
| *3* | 4% $D_2O$ | 20 | $\delta$[a]) [ppm] | 8.43 (*s*) | 7.50 (*d*, *J* = 8.4 Hz) | 6.44 (*d*, *J* = 8.4 Hz) | 4.19 (br. *s*) | 4.29 (*dd*, *J* = 8.0, 4.7 Hz) | 2.32 (*m*) | 2.13 (*m*), 2.04 (*m*) |
| | | | $T_1$ [s] | 1.20±0.01 | 1.10±0.02 | 0.63±0.02 | | | 0.35±0.05 | 0.27±0.02, 0.27±0.02 |
| *4* | 4% $D_2O$, 1M NaCl | 20 | $\delta$[b]) [ppm] | 8.29 | 7.50 | 6.48 | 4.11 | 4.29 | 2.36 | 2.00–2.24 |
| | | | $T_1$ [s] | 0.78±0.04 | 0.86±0.04 | 0.59±0.01 | | | 0.31±0.05 | 0.25±0.03, 0.25±0.03 |

[a]) 4% in $H_2O/D_2O$ 9:1: $\delta(H_i) = 8.01$ (*d*, *J* = 6.75 Hz), $T_1 = 0.25\pm0.02$.
[b]) 4% in $H_2O/D_2O$ 9:1, 1M NaCl: $\delta(H_i) = 8.03$, $T_1 = 0.29\pm0.02$.

folate solutions in $H_2O/D_2O$ 9:1, with and without NaCl (1M), corresponding to the amidic proton $H_i$ of the 4-aminobenzoyl moiety, on the basis of the data obtained from a 2D-COSY spectrum.

*Chemical Shifts.* In *Table 2*, the first set of results measured at 60° on a 0.4% $D_2O$ solution refers to the free form of $Na_2$fol (*Entry 1*). The same solution at room temperature (*Entry 2*) already shows the formation of an assembled species, as pointed out by CD spectroscopy, and displays very sharp signals, some of which are shifted towards low frequencies; the larger shifts concern protons belonging to the aromatic core, while the chemical shifts of the aliphatic dicarboxylic chain are nearly unchanged. The general trend of multiplicity and sharpness of signals observed in the previous spectra do not change at higher concentrations (*Entry 3*), while chemical shift values of $H_h$, $H_g$, $H_f$, and $H_e$ undergo a further decrease (0.11–0.27 ppm). The situation changes dramatically when an electrolyte such as NaCl is added to the 4% solution (*Entry 4*); the signals are still strong but broader, and the multiplicity is lost; $H_h$ undergoes a further shielding effect.

In brief, the self-assembling of $Na_2$fol leads to a general shielding effect which is stronger for the heterocyclic nucleus and for its neighboring protons and becomes weaker as the protons move away from the aromatic core of the aggregate.

$T_1$ *Values.* The effect of temperature change on the longitudinal relaxation rate values is rather strong, as estimated from standard equations relating $1/T_1$ *vs.* $\tau_c$ and $\tau_c$ *vs.* *T* [16]. It is, therefore, not possible to evaluate correctly the contribution of the self-assembly process occurring between 60 and 20° (*Entries 1* and *2*) to the $T_1$ values. On the contrary, the result of a concentration increase from 0.4 to 4% (*Entries 2* and *3*) at room tempera-

ture is a marked decrease of the relaxation time of $H_h$, and a constancy of the relaxation rates of the other protons. This picture denotes that the degree of association of the pterin nucleus is increasing in this range of concentration. The addition of NaCl (*Entry 4*) causes a further decrease of the relaxation times of some protons ($H_h$, $H_g$, and $H_f$ to some extent), and this suggests that the present structure is constituted by a different aggregate than the preceding one (*Entry 3*), as confirmed by CD and SANS spectroscopies.

At lower temperature (down to 4°), the spectral signal become weak and very broad, indicating the formation of higher associated states of the aggregates.

2.3.2. *2D-NMR Data. Fig. 7* represents a phase-sensitive 2D-NOESY spectrum of a 4% (*w*/*w*) $Na_2$fol solution in $D_2O$ in the presence of NaCl (1M), using a mixing-time value of 200 ms. This spectrum is characterized by intense cross-peaks of the same sign as the diagonal ones (negative NOE regime $\omega\tau_c > 1$), indicative of the existence of aggregated molecules. A series of measures were obtained for this solution using different mixing-time values ($\tau_m$ 50, 75, 100, 150, 200, 250, 300 ms) to identify the effects of anomalous enhancements due to spin diffusion by their non-exponential build-up. In this range of values, the build-up curve relative to the aromatic protons ($H_f$ and $H_g$) is approximately linear until $\tau_m$ 250 ms. Analogous linear plots can be drawn for enhancements due to direct NOE linking the protons $H_e$ with $H_h$ and $H_a$ or $H_b$ with $H_d$. The observation of indirect NOE's connecting $H_g$ with $H_e$ and $H_g$ with $H_d$, at 100 and 150 ms, is due to the spin-diffusion pathways caused by $H_f$ and the amidic proton $H_i$, respectively. Enhancements relative to protons $H_h/H_f$, $H_h/H_g$, and $H_d/H_g$ appear only in spectra measured at $\tau_m$ 100 and 150 ms. The NOESY data obtained for a 4% $Na_2$fol solution in 1M NaCl in $H_2O/D_2O$ 9:1 ($\tau_m$ 100 and 200 ms) allow the detection of an additional cross-peak due to the proximity of $H_i$ and $H_g$.

The phase-sensitive 2D-NOESY spectrum obtained for a folate solution in 100% $D_2O$ shows cross-peaks of minor intensity; in addition, the indirect NOE enhancements relative to protons $H_g$ with $H_d$ and $H_g$ with $H_e$ are absent. These data resemble those obtained by a 1D steady-state NOE difference experiment carried out at 60° on a 0.4% folate solution (free molecule). Also the free folate show the same connections through space already seen in the kinetic NOE experiments of the aggregates discussed above; in particular the interesting interactions $H_h/H_i$, $H_h/H_g$, and $H_e/H_f$ are detected.

Mixing time values of 200 and 300 ms were chosen for the evaluation of the average interproton distances of folate in 1M NaCl and in 100% $D_2O$ solutions, respectively (*Table 3*).

As the proton distances experimentally calculated for the two aggregates (with and without NaCl) are not very different from those obtained for the free molecule, we believe that the conformation assumed by the monomer at 60° is partially maintained in the aggregate. The detection of spin-diffusion phenomena, revealed in the NOESY spectra of the NaCl aggregate, indicates a structure of greater extension than that of the non-NaCl aggregate; this structure is likely to be moderately blocked also for the protons of the aliphatic chains belonging to contiguous layers. On the contrary, the aggregate without NaCl is likely to be composed of a rigid core (the pterin moieties bound together), a more flexible part (the 4-aminobenzoyl function), and a mobile dicarboxylic chain, presumably characterized by various local correlation times.

An experimental estimate of the $\tau_c$ value from 2D-NOESY measurements is obtained rearranging *Eqn. 3* which describes the dipolar interaction between two nuclei A and B as

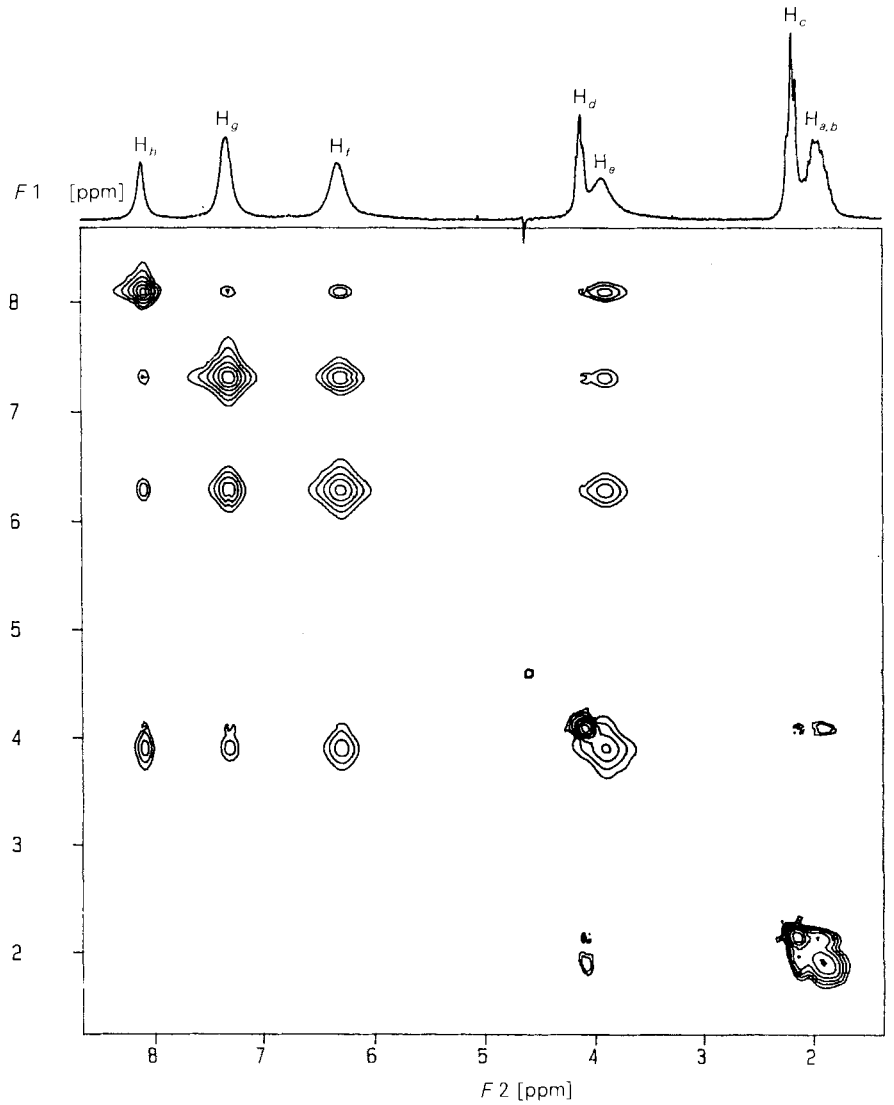


Fig. 7. *$^1$H-NOESY Spectrum* (mixing time 200 ms) *at 200 MHz of a 4% (w/w) $Na_2$fol solution in $D_2O$ in the presence of NaCl* (1M) *at 20°*. All cross-peaks shown correspond to positive NOE's, $^1$H-signals of the 1D $^1$H-NMR spectrum at the top of the contour plot are labelled according to *Fig. 1a*.

Table 3. *Average Interproton Distances* [Å] *Calculated from NOESY and 1D-NOE Steady-State Difference Experiments*

| *Entry* | $Na_2$fol | *T* | $H_h/H_e$ | $H_h/H_f$ | $H_h/H_g$ | $H_e/H_f$ | $H_g/H_i$ [a]) | $H_{a,b}/H_d$ | $H_c/H_d$ |
|---|---|---|---|---|---|---|---|---|---|
| *1* | 4% $D_2O$ [b]), 1M NaCl | r.t. | 2.64–2.90 | 3.26–3.47 | 3.67–3.87 | 2.47–2.62 | 2.50–2.64 | 2.95–3.54 | 2.95–3.20 |
| *2* | 4% $D_2O$ [c]) | r.t. | 2.90–3.26 | 3.26–3.39 | 3.10–3.23 | 2.75–3.19 | | 2.94–3.12 | 2.50–3.04 |
| *3* | 0.4% $D_2O$ | 60° | 3.00–3.20 | 3.00–3.75 | 3.25–3.50 | 2.88–3.00 | | 2.49–3.03 | 2.52–3.06 |

[a]) $H_2O/D_2O$ 9:1, $\tau_m$ 200 ms. [b]) $\tau_m$ 200 ms. [c]) $\tau_m$ 300 ms.

a function of the mixing time, with $J(n\omega) = \tau_c/[1 + (n\omega\tau_c)^2]$ and $q = 0.1\,\gamma^4(h/2\pi)^2(\mu_0/4\pi)^2$, where $I_{AB}$ and $I_{AA}$ represent the cross and diagonal peak integrated intensities at $\tau_m \neq 0$ and $\tau_m = 0$, respectively; $r$ is the internuclear distance, and the physical constants have their usual meanings. The calculation of $\tau_c$ was carried out using the known distance of the aromatic *ortho* protons ($r = 2.50$ Å), which is likely to reflect the correlation time of the whole molecule; the values obtained are $5 \cdot 10^{-9}$ and $1.5 \cdot 10^{-9}$ s for a 4% (*w*/*w*) $Na_2$fol solution in $D_2O$ with and without added salt, at $\tau_m$ 200 and 300 ms, respectively.

$$I_{AB}/I_{AA} = |qr^{-6}[6J(2\omega) - J(0)]|\tau_m \tag{3}$$

The corresponding values of $\omega\tau_c$ indicate that the two kinds of aggregates tumble at a rate differing from the zero-crossing point one ($\omega\tau_c = 1.12$); in particular, the NaCl aggregate shows larger NOE enhancements, as pointed out by its higher value of $\omega\tau_c$ (6.3), than those detected for the associated folate without added salt ($\omega\tau_c = 1.9$). For the latter aggregate, if different local tumbling rates occur, the value of $\omega\tau_c$ very close to the zero-crossing point may explain the lack of some cross-peaks in the spectra. On the basis of these arguments and also considering the lower $\tau_c$ value, we believe that smaller, as well as less compact aggregates, are present in solutions free from NaCl.

A theoretical prediction of the correlation time of a molecule considered as a sphere of radius $a$ in isotropic tumbling is given by the *Debye* equation (*Eqn. 4*) in which $\tau_c$ depends on the microscopic viscosity $\eta$ of the solvent ($1 \cdot 10^{-3}$ Pa s for water) and on the size of the molecule ($a^3$). Using the value of the radius of the molecule $a = 15.5$ Å, obtained considering an aggregate composed of a stack of ten tetramers of 35 Å height (see *Sect. 2.1*), the correlation time results to be $4 \cdot 10^{-9}$ s.

$$\tau_c = 4\pi\eta a^3/3kT \tag{4}$$

The comparison between the experimental and the theoretical $\tau_c$ values obtained for the NaCl aggregate shows that the assumptions of the molecular structure present in solution, made on the basis of SANS experiments, are in reasonable agreement with the NMR data.

**3. Conclusions.** – From the study of the cholesteric and hexagonal liquid crystalline phases [4] [5], a structural model for the self-assembled folates in water was proposed: the aggregates are cylindrical and of finite length, composed of a stacked array of folate tetramers; each tetramer is formed by *Hoogsteen*-bonded folate residues. In pure water, the tetramer-tetramer interaction is weak, and the length of aggregates increases slowly with the folate concentration. In the presence of NaCl, the tetramer-tetramer interaction is stronger, and the column length is significant also at relatively low folate concentrations: *ca.* 20 disks at the isotropic-cholesteric transition (27% (*w*/*w*)).

With the present experiments, different types of aggregation could be formulated; however, considering the unambiguous presence of tetramer-based columnar aggregates in the liquid crystalline aqueous phase, we think it is reasonable to extend this model also to more diluted aqueous solutions. Using this model, SANS experiments indicate the presence of cylindrical aggregates (*ca.* 9 disks) only at a relatively high concentration (4% (*w*/*w*)) in the presence of an excess of $Na^+$ or $K^+$ ions. Under the same experimental conditions, CD spectra indicate the presence of an assembled species (form **II**); also at a

lower concentration (0.4% (*w*/*w*)), a very similar CD spectrum is observed, indicating the same basic structure and a smaller length or concentration.

In pure water, CD spectra indicate the presence of assembled species (form **I**) different from form **II**. This aggregate is not detectable by SANS and, therefore, must be shorter than the corresponding form **II**. The different CD spectra observed in the aromatic region indicate a different configuration of the aromatic core. Considering that the hexagonal phase observed in pure water is also formed by cylindrical aggregates, but with a weak interaction between tetramers, we think that a similar structure should be assigned to form **I**.

NMR Data confirm this picture: the aggregation generates a proton shielding and a concomitant decrease of longitudinal relaxation times which is more pronounced for the aromatic part of the folate. In addition, chemical shifts remain nearly constant, and $T_1$ values are shorter in passing from the 'non-NaCl' to the 'NaCl' aggregate, indicating that forms **I** and **II** are substantially similar and the latter is the largest one.

Both CD and NMR data also show that the glutamic chains are rather mobile in both aggregates. 1D- and 2D-NOE measurements allow one to define a possible conformation of the monomer in solution through the evaluation of the inter-proton distances; this analysis indicates that the configuration of folate does not change much when passing from the free molecule to the assembled species.

Finally, NOESY data give an estimate of the tumbling rates of these species in solution which is in agreement with the cylindrical model proposed.

We would like to thank Prof. *Claudio Luchinat*, University of Bologna, for helpful discussions of the NMR data. We are grateful to *CNR* and *MURST* for support of this research.

## Experimental Part

*Small-Angle Neutron-Scattering Experiments.* Small-angle neutron-scattering experiments were performed at the *LOQ* diffractometer of the *Rutherford Appleton Laboratory*; Didcot, UK. A neutron beam with a wavelength varying from 2 to 10 Å was used; a two-dimensional detector (64 × 64 $cm^2$) was situated 4.4 m from the sample, allowing investigation of a range of $Q$ (the scattering vector $Q$ being defined as $(4\pi \sin\theta)/\lambda$, where $2\theta$ is the scattering angle) from 0.015 to 0.20 $Å^{-1}$, using the time-of-flight technique. To obtain good statistics, a typical run time of 6 h was chosen. The raw data were corrected for electronic-noise and sample-holder signal by measuring a cadmium sample and an empty quartz cell, respectively. The samples were measured in 2-mm-thick quartz cells at 25 and 10°. The temperature was controlled with an accuracy of 1° by using a circulation thermostat.

To improve the statistics, $D_2O$ was used as solvent. Two important points must be made: first, to calculate the mean particle-scattering length, we assumed that all the labile H-atoms in the folate molecule exchange with the solvent, as observed for polynucleotide derivatives [13]. The second point concerns the fact that the aggregation phenomena could be different in normal and heavy water. It is well known in fact that $D_2O$ may stabilize hydrophobic interactions: therefore, the investigated samples were analyzed by optical polarized microscopy before SANS experiments to verify that they were in the isotropic phase.

Concerning the data analysis, in the case of a two-phase model with identical scattering centres and random orientation, the coherent macroscopical differential cross section of a sample is related to the scattering-centre parameters by *Eqns. 5* [11], where $N$ is the number of scattering particles per unit volume, $\Sigma b$ the sum of the scattering length of all the nuclei of the whole scattering particles, $\rho_s$ the scattering-length density of the solvent, $V$ the scattering-particle volume, and $|F(Q)|^2$ the squared averaged form factor, which depends on the size and shape of the scattering particles. At low $Q$, the form factor can be approximated by the so-called *Guinier* law [9] [11]; *i.e. Eqn. 6*, where $R_g$ is the gyration radius defined by *Eqn. 7*, and $d\Sigma/d\Omega(0)$ is the coherent intensity scattered at $Q = 0$. Considering that $F(0) = 1$, *Eqn. 8* follows.

$$d\Sigma/d\Omega(Q) = N(\Sigma b - \rho_s V)^2 |F(Q)|^2 \quad (5)$$

$$d\Sigma/d\Omega(Q) = d\Sigma/d\Omega(0) \exp(-Q^2 R_g^2/3) \quad (6)$$

$$R_g^2 = \Sigma_j((\rho(r_j) - \rho_s) V_j r_j^2)/\Sigma_j((\rho(r_j) - \rho_s) V_j) \quad (7)$$

$$d\Sigma/d\Omega(0) = N(\Sigma b - \rho_s \cdot V)^2 \quad (8)$$

Due to the impossibility of discriminating the SANS signal from the primary beam at low $Q$ and from the background at large $Q$, a measurement can only investigate over a finite $Q$ range. If the *Guinier* law is satisfied ($Q_{max} R_g < 1.5$), the gyration radius $R_g$ and the $d\Sigma/d\Omega(0)$ value can be obtained by a linear fit of the experimental SANS data in the so-called *Guinier* plot [9] [11] $\ln(d\Sigma/d\Omega(Q))$ *vs.* $Q^2$. Likewise, in the case of needle-like particles, from the *Guinier* plot $\ln(d\Sigma/d\Omega(Q)\, Q)$ *vs.* $Q^2$, the cross-sectional intensity scattered at zero angle and the gyration radius of the cross section of the scattering particle $R_c$ can be determined [6] [8] [9].

*Circular Dichroism.* CD Experiments were performed with a *Jasco J710* spectropolarimeter equipped with a *Heto/Hetofrig* circulating thermostat using 0.01–0.001-cm path-length cells with thermostatting jackets. Data were handled with a mathematic noise-reduction routine (*Jasco* software).

*NMR Measurements.* All the NMR data were recorded on a *Varian-Gemini-200* spectrometer; $^1$H-chemical shifts at r.t. and at 60° are referred to $H_2O$ (4.81 and 4.41 ppm, resp.). 1D Spectra were measured on 0.4 and 4% (*w/w*) disodium folate ($Na_2$fol) solns. in $D_2O$ and in $H_2O/D_2O$ 9:1 in the absence and in the presence of NaCl (1M), at temp. from 4 to 75°. Spectra in $H_2O$ were acquired using either presaturation or a $\bar{1}33\bar{1}$ pulse sequence [17] for water suppression; in neither case could NH signals be detected. A 1D-NOE steady-state difference experiment was carried out on a 0.4% (*w/w*) $Na_2$fol soln. in $D_2O$ at 60°. A 2D-COSY spectrum of a 4% (*w/w*) $Na_2$fol soln. in 1M NaCl was carried out to ascertain the assignment of all the protons detected. Phase-sensitive 2D-NOESY spectra were recorded for 4% (*w/w*) $Na_2$fol solns. in $D_2O$ and in $H_2O/D_2O$ 9:1 with and without added salt. The instrumental settings were: spectral width 3 kHz, pulse width 25 μs (*ca.* 90° flip angle), repetition time 1.5–3 s, complex data points in $t_2$ 1024, complex FIDs in $t_1$ 256, number of transients 16.

## REFERENCES


[1] J.-M. Lehn, *Angew. Chem. Int. Ed.* **1988,** *27,* 89; *ibid.* **1990,** *29,* 1304; J.-M. Lehn, 'Supramolecular Chemistry', VCH, Weinheim, 1995.

[2] D. Sen, W. Gilbert, *Nature (London)* **1988,** *334,* 364; W.I. Sundquist, A. Klug, *ibid.* **1988,** *342,* 825; R. Jin, K.J. Breslauer, R.A. Jones, B.L. Gaffney, *Science* **1990,** *280,* 543; I.G. Panyutin, O.I. Kovalsky, E.I. Budowsky, R.E. Dickerson, M.E. Rikhirev, A.A. Lipanov, *Proc. Natl. Acad. Sci. U.S.A.* **1990,** *87,* 867; D. Sen, W. Gilbert, *Nature (London)* **1990,** *344,* 410; A.M. Zahler, J.R. Williamson, T.R. Cech, D.M. Prescott, *ibid.* **1991,** *350,* 718; C.C. Hardin, E. Henderson, T. Watson, J.K. Prosser, *Biochemistry* **1991,** *30,* 4460; F.W. Smith, J. Feigon, *Nature (London)* **1992,** *356,* 164; P. Balagurumoorthy, S.K. Brahmachari, D. Mohanty, M. Bansal, V. Sasisekharan, *Nucleic Acids Res.* **1992,** *20,* 4061; D. Sen, W. Gilbert, *Biochemistry* **1992,** *31,* 65; Y. Wang, D.J. Patel, *ibid.* **1992,** *31,* 8112; C. Kang, X. Zhang, R. Ratliff, R. Moyzis, A. Rich, *Nature (London)* **1992,** *356,* 126; M. Lu, Q. Guo, N.R. Kallenbach, *Biochemistry* **1993,** *32,* 598; E.A. Venczel, D. Sen, *ibid.* **1993,** *32,* 6220; G. Gupta, A.E. Garcia, Q. Guo, M. Lu, N.R. Kallenbach, *ibid.* **1993,** *32,* 7098; F.W. Smith, J. Feigon, *ibid.* **1993,** *32,* 8682; W.I. Sundquist, S. Heaphy, *Proc. Natl. Acad. Sci. U.S.A.* **1993,** *90,* 3393; H. Deng, W.H. Braunlin, *Biopolymers* **1995,** *35,* 677.

[3] G.P. Spada, A. Carcuro, F.P. Colonna, A. Garbesi, G. Gottarelli, *Liq. Cryst.* **1988,** *3,* 651; P. Mariani, C. Mazabard, A. Garbesi, G.P. Spada, *J. Am. Chem. Soc.* **1989,** *111,* 6369; G.P. Spada, P. Mariani, G. Gottarelli, A. Garbesi, S. Bonazzi, M.G. Ponzi Bossi, M.M. De Morais, M. Capobianco, *ibid.* **1991,** *113,* 5809; S. Bonazzi, M.M. De Morais, A. Garbesi, G. Gottarelli, P. Mariani, G.P. Spada, *Liq. Cryst.* **1991,** *10,* 495; L.Q. Amaral, R. Itri, P. Mariani, R. Micheletto, *ibid.* **1992,** *12,* 913; A. Garbesi, G. Gottarelli, P. Mariani, G.P. Spada, *Pure Appl. Chem.* **1993,** *65,* 641; P. Mariani, M.M. De Morais, G. Gottarelli, G.P. Spada, H. Delacroix, L. Tondelli, *Liq. Cryst.* **1993,** *15,* 757; G. Gottarelli, G.P. Spada, A. Garbesi, in 'Comprehensive Supramolecular Chemistry', Vol. 9, 'Templating, Self-Assembly and Self-Organization', Eds. J.-M. Lehn, J.L. Atwood, D.D. MacNicol, J.A.D. Davies, F. Vogtle, J.-P. Sauvage, and M.W. Hosseini, Pergamon Press, Oxford, 1995, in press.

[4] S. Bonazzi, M. M. De Morais, G. Gottarelli, P. Mariani, G. P. Spada, *Angew. Chem. Int. Ed.* **1993,** *32,* 248.
[5] F. Ciuchi, G. Di Nicola, H. Franz, G. Gottarelli, P. Mariani, M. G. Ponzi Bossi, G. P. Spada, *J. Am. Chem. Soc.* **1994,** *116,* 7064.
[6] F. Carsughi, M. Ceretti, P. Mariani, *Eur. Biophys. J.* **1992,** *21,* 155.
[7] C. L. Fisk, E. D. Becker, H. T. Miles, T. J. Pinnavaia, *J. Am. Chem. Soc.* **1982,** *104,* 3307.
[8] O. Kratky, in 'Biophysics', Eds. W. Hoppe, H. M. Lohmann, and H. Ziegler, Springer-Verlag, Berlin, 1983, pp. 65–74.
[9] S. H. Chen, T. L. Lin, in 'Methods in Experimental Physics', Vol. 23, 'Neutron, Scattering', Part. B, Eds. R. Celotta, J. Levine, D. L. Price, and K. Skold, Academic Press, San Diego, 1987, pp. 489–543.
[10] O. Kratky, P. Laggner, in 'Encyclopedia of Physics, Science and Technology', Academic Press, San Diego, 1987, Vol. 14, pp. 693–742.
[11] A. Guiner, G. Fournet, 'Small Angle Scattering of X-Rays', Wiley, New York, 1955.
[12] B. Jacrot, *Rep. Prog. Phys.* **1976,** *39,* 911.
[13] B. Jacrot, G. Zaccai, *Biopolymers* **1981,** *20,* 2413.
[14] W. Saenger, 'Principles of Nucleic Acid Structure', Springer, New York, 1984, p. 317.
[15] C. W. Hilbers, in 'Biological Applications of Magnetic Resonance', Ed. R. G. Shulman, Academic Press, New York, 1979, pp. 1–43.
[16] D. Neuhaus, M. P. Williamson, 'The Nuclear Overhauser Effect in Structural and Conformational Analysis', VCH, New York, 1989.
[17] P. J. Hore, *J. Magn. Reson.* **1983,** *55,* 283.